HHS Public Access

Author manuscript

Nat Mater. Author manuscript; available in PMC 2015 December 01.

Published in final edited form as:

Nat Mater. 2015 October ; 14(10): 1040–1048. doi:10.1038/nmat4357.

Unjamming and cell shape in the asthmatic airway epithelium

Jin-Ah Park[1,*,†], **Jae Hun Kim**[1,†], **Dapeng Bi**[2], **Jennifer A. Mitchel**[1], **Nader Taheri Qazvini**[1,3], **Kelan Tantisira**[4], **Chan Young Park**[1], **Maureen McGill**[1], **Sae-Hoon Kim**[1], **Bomi Gweon**[1], **Jacob Notbohm**[1], **Robert Steward Jr**[1], **Stephanie Burger**[1], **Scott H. Randell**[5], **Alvin T. Kho**[6], **Dhananjay T. Tambe**[1,7], **Corey Hardin**[1], **Stephanie A. Shore**[1], **Elliot Israel**[4], **David A. Weitz**[8], **Daniel J. Tschumperlin**[9], **Elizabeth P. Henske**[4], **Scott T. Weiss**[4], **M. Lisa Manning**[2], **James P. Butler**[1,4], **Jeffrey M. Drazen**[1], and **Jeffrey J. Fredberg**[1]

[1]Harvard T.H. Chan School of Public Health, Boston, Massachusetts 02115, USA

[2]Syracuse University, Syracuse, New York 13244, USA

[3]School of Chemistry, College of Science, University of Tehran, Tehran 14179, Iran

[4]Brigham and Women's Hospital, Harvard Medical School, Boston, Massachusetts 02115, USA

[5]The University of North Carolina at Chapel Hill, Chapel Hill, North Carolina 27514, USA

[6]Children's Hospital, Boston, Massachusetts 02215, USA

[7]Department of Mechanical Engineering, University of South Alabama, Mobile, Alabama 36688, USA

[8]Harvard University, Cambridge, Massachusetts 02138, USA

[9]Mayo Clinic College of Medicine, Rochester, Minnesota 55905, USA

Abstract

From coffee beans flowing in a chute to cells remodelling in a living tissue, a wide variety of close-packed collective systems— both inert and living—have the potential to jam. The collective can sometimes flow like a fluid or jam and rigidify like a solid. The unjammed-to-jammed transition remains poorly understood, however, and structural properties characterizing these

Correspondence and requests for materials should be addressed to J.-A.P. jpark@hsph.harvard.edu.
[†]These authors contributed equally to this work.

Author contributions

J.-A.P. designed experiments, carried out time-lapse imaging of HBECs in ALI culture and interpreted data. J.H.K. designed measurements of physical forces within HBECs and analysed data. J.H.K. and M.M. carried out force-measurement experiments. J.H.K., N.T.Q., C.Y.P. and C.H. analysed the dynamics of cellular motions. D.B. and J.A.M. analysed cell-shape parameters. D.B. modelled cell-shape parameters and cell motility. J.A.M. and S.-H.K. carried out time-lapse imaging of HBECs in ALI culture. D.T.T., B.G., J.N., R.S. and S.B. contributed to preparation of physical-force measurements. S.H.R. contributed to the design of experiments and provided primary HBECs. D.A.W., D.J.T., S.T.W., M.L.M., J.P.B., J.M.D. and J.J.F. guided data interpretation and analysis of cellular migration and the jamming transition. S.H.R., A.T.K., S.A.S., E.I., S.T.W., E.P.H., K.T. and J.M.D. guided data interpretation on the biological relevance of cellular migration. J.-A.P., J.H.K., D.B., M.L.M. and J.J.F., wrote the manuscript. J.-A.P. and J.J.F. oversaw the project.

Additional information

Supplementary information is available in the online version of the paper.

Competing financial interests

The authors declare no competing financial interests.

phases remain unknown. Using primary human bronchial epithelial cells, we show that the jamming transition in asthma is linked to cell shape, thus establishing in that system a structural criterion for cell jamming. Surprisingly, the collapse of critical scaling predicts a counter-intuitive relationship between jamming, cell shape and cell–cell adhesive stresses that is borne out by direct experimental observations. Cell shape thus provides a rigorous structural signature for classification and investigation of bronchial epithelial layer jamming in asthma, and potentially in any process in disease or development in which epithelial dynamics play a prominent role.

One of the central unresolved mysteries of asthma is how the asthmatic airway remodels itself[1]. This remodelling is often progressive and has long been thought to be the end product of a cascade of cell-signalling events that are initiated in the bronchial epithelium and driven by repetitive inflammatory, allergic, or viral insults[1]. Tissue-remodelling events more broadly, including those underlying morphogenesis, wound repair and cancer invasion, have been linked to collective cellular migration[2–5], often in the context of the epithelial-to-mesenchymal transition (EMT; ref. 6). But no clear physical picture has yet emerged that can capture these collective biological processes and their interconnections. Here we provide evidence that the physical process of cell jamming and unjamming[5,7–11], which has been missing from descriptions of tissue remodelling, might tie together at least some of them.

Primary human bronchial epithelial cells (HBECs) were derived from non-asthmatic and asthmatic donors, plated on a porous Transwell insert, and established in air/liquid interface (ALI) culture[12] (Methods). Initial culture in submerged conditions causes basal cells to proliferate, and subsequent culture in ALI conditions inhibits any further proliferation and triggers differentiation of those basal cells into a mature confluent pseudostratified bronchial epithelial layer comprising goblet cells and ciliated cells[13]. Here we show that such a pseudostratified layer derived from non-asthmatic donors is quiescent. Cellular motions are relatively small, cellular rearrangements among neighbouring cells are rare, and each cell remains virtually caged by those immediate neighbours. Statistical analyses of these motions confirm that such a layer is solid-like and jammed. However, application of an apical-to-basal mechanical stress mimicking the compressive effect of bronchospasm[12,14,15] (Supplementary Fig. 1) is sufficient to trigger large cellular motions and cooperative cellular rearrangements. Cells move chaotically, but the motions exhibit cooperative packs and swirls; such a layer is fluid-like and unjammed. We then examine the more complex process of progressive layer maturation, where we find an innate tendency of the maturing layer to transition from an immature, fluid-like, unjammed phase in which cells readily rearrange and flow, into a mature, solid-like, jammed phase in which cells become virtually frozen in place[8,9,16]. As compared with non-asthmatic donors, however, in the maturing layer derived from asthmatic donors this jamming transition is delayed substantially or disrupted altogether. In all these cases, the transition between unjammed and jammed phases is continuous; as the cell layer approaches the jamming transition, cellular motions become progressively slower, pack sizes become progressively larger, and pack lifetimes become progressively longer.

One might have expected that cell jamming would be caused by increasing mutual cell–cell adhesive stresses such that cells become stuck to immediate neighbours and, as a result, the

cellular collective rigidifies, the mutual cellular rearrangements stop, and the constituent cells cannot move[17]. Much to our surprise, direct measurements defied this expectation—in layers that become jammed, the adhesive stresses between a cell and its neighbours were attenuated, not augmented. To explain this paradox, we turned to the well-known vertex model, wherein a competition between cell–cell adhesive stresses and cell cortical tension control changes of cell shape[18–20]. Novel analysis of this model, including a critical scaling analysis, predicts that increased adhesion leads to increased fluidity, and that cell jamming occurs as a well-defined index of cell shape approaches a critical value. We show that the shape index acts as a simple structural order parameter that takes on different values on either side of the jamming transition. Using that shape index, we show not only that cell shape in the bronchial epithelial layer differs between cells derived from non-asthmatic versus asthmatic donors, but also that, regardless of cell origin, cell shape at the jamming transition matches theoretical predictions, and thus resolves the paradox. This new physical picture raises questions about the relationship between the epithelial-to-mesenchymal transition and unjamming and, conversely, between the mesenchymal-to-epithelial transition and jamming. Similarly, it suggests new, testable hypotheses concerning asthma aetiology and asthma therapy. The more fundamental significance of these findings, however, may be to broaden notions of jammed matter and generalize understanding of jamming mechanisms.

Compression unjams the jammed HBEC layer

Mechanical compression of the bronchial epithelium occurs during severe bronchospasm (Supplementary Fig. 1) and is sufficient to induce maladaptive airway remodelling even in the complete absence of inflammatory events[14,15]. Although certain cell-signalling modules have been identified, such as autocrine signalling through the epidermal-growth-factor-receptor family of ligands, the physical mechanism remains unclear. To trigger these events we followed the protocol of ref 14; on day 16 of ALI culture we exposed the HBEC layer to a compressive apical-to-basal stress, P, spanning the physiologic range (0, 3, 10, 20, or 30 cm H_2O; Fig. 1 and Supplementary Fig. 1), where 3 cm H_2O corresponds roughly to the maximal compressive stress expected to be exerted on HBECs by quiet tidal breathing, and 30 cm H_2O corresponds to that expected during severe bronchospasm[21,22].

The manner in which a cell moves provides clues about mechanisms that promote or impede its mobility (Fig. 1a). Therefore, we began by quantifying cellular motions using their mean square displacement (MSD) over a given time interval, Δt, averaged over many cells in several optical fields (Methods). In many physical systems, the MSD increases with time as a power law, Δt^{α}, where the exponent α is determined empirically. When the exponent is unity ($\alpha = 1$), as in uncorrelated random Brownian motion, particle motions are diffusive. When $\alpha < 1$, particle motions are sub-diffusive, as when a particle might, in time, escape the cage comprising its immediate neighbours only to become quickly recaged by its new immediate neighbours; this uncaging–recaging process thereupon repeats in a stochastic fashion. When $\alpha > 1$, particle motions are super-diffusive, and when $\alpha = 2$, as occurs in simple linear translation at constant velocity, motions are ballistic.

In HBECs from non-asthmatic donors in ALI culture, cellular motions were smallest when the compressive stress, P, was zero and increased systematically as P was increased (Fig. 1b

and Supplementary Movie 1). When Δt was small and P was zero, the MSD increased slowly with time in a sub-diffusive manner as if each cell were caged or jammed by its immediate neighbours. But as Δt exceeded 10min the MSD grew as $\Delta t^{1.3}$, indicating that motions at longer times were slightly super-diffusive, and suggesting that each cell was eventually able to escape its cage and move in a persistent direction. But as P was increased progressively to 30 cm H_2O, the MSD at the highest P increased by about two orders of magnitude and varied as $\Delta t^{1.8}$. Cells in this compressed state were seen to become highly mobile and strongly super-diffusive (Fig. 1b).

These swirling cellular motions and their changes were visually striking (Supplementary Movie 1). To provide further quantitative characterization of these motions, we measured the fractional change of cellular position in a given time increment Δt. Much as is done conventionally in studies of cooperative particle motions in jammed or glassy inert systems[23], here we chose 15% of average particle (that is, cellular) diameter as the reference length scale; if a region moved less than 15% of the average cellular diameter over the time interval Δt, we considered this as 100% overlap with the initial position, whereas if a region moved more than 15% of a cellular diameter, we considered this as 0% overlap (Methods). The average value of this overlap function over the entire optical field was defined as $Q(\Delta t)$ (ref. 23) and the ensemble average over all sequence images, ($\langle Q(\Delta t)\rangle$, was computed. Uncompressed cells and those compressed with P less than 20 cm H_2O showed nearly perfect overlap ($\langle Q(\Delta t)\rangle = 1$) for as much as 144min, as if cells were immobile and jammed. However, for cells compressed with P of 30 cm H_2O, $\langle Q(\Delta t)\rangle$ fell to 0.17 at 144min (Fig. 1c), suggesting appreciable mobility and, potentially, unjamming.

The MSD and the overlap function Q are useful metrics of cellular motions. However, these metrics by themselves fail to distinguish uncorrelated cellular motions from the cooperative motions that comprise the strings, clusters, swirls or eddies that are the hallmark of the structurally heterogeneous dynamics and typify jammed matter close to a jamming transition[16,24]. In such systems, as the jamming transition is approached, the cooperativity of these motions increases and, as a result, the length scale and the timescale of these motions tend to grow sharply[23,25,26]. Therefore, from the overlap function $Q(\Delta t)$ we computed the four-point susceptibility, $\chi_4(\Delta t)$, which exhibits a peak whose position corresponds roughly to pack or swirl lifetime and whose magnitude corresponds roughly to pack or swirl size (Methods)[4,24,27]. Accordingly, after several pack lifetimes a sufficient degree of structural rearrangements will have occurred such that any individual cell will find itself surrounded by a different set of immediate neighbours, and the original pack will have become shuffled with its neighbours to the extent that it becomes unrecognizable. As in the well-established glass transition[28], there is no objective cutoff that defines a jamming transition; rather, the transition is continuous, and jamming is said to occur when pack lifetime grows to exceed the laboratory measurement window, which we take here as 144 min.

In HBEC layers derived from non-asthmatic donors, $\chi_4(\Delta t)$ revealed no peak for P less than 20 cm H_2O and time intervals less than 144 min (Fig. 1d); if a peak exists at all in these cases, it must be for substantially longer times. However, for P = 30 cm H_2O, a well-defined peak in $\chi_4(\Delta t)$ emerged, corresponding to faster-moving cooperative packs comprising roughly seven cells with an average pack lifetime of 42 min (Fig. 1d). Compressive stress of

30 cm H_2O pressure was therefore sufficient to unjam the layer comprised of HBECs from non-asthmatic donors, whereas at lower compressive stresses the induced motions were far smaller, and structurally heterogenetic dynamics was not evident, as if the layer were frozen.

In cells from asthmatic donors, jamming is delayed

In submerged conditions, primary HBECs grow until confluence and, subsequently, in ALI culture they differentiate without further proliferation. These events recapitulate repair processes that are known to occur *in vivo* following epithelial injury or sloughing[13]. Roughly by day 3 in ALI culture the early phase of rapid proliferation was completed and the maturation and differentiation of the layer then continued; cell densities varied from well-to-well and from donor-to-donor, ranging roughly from 4,700 to 5,300 cells mm^{-2} and averaging 5,116 ± 233 cells mm^{-2}, but did not increase systematically with ALI day (p = 0.37). The cell layer increasingly exhibited a well-differentiated pseudostratified phenotype that included goblet cells and ciliated cells, apicobasal polarization, tight junctions, and an increasingly tight barrier function, as reflected in progressive increases of the trans-epithelial electrical resistance (TEER; ref. [29]). As shown previously in HBECs (refs 29, 30), we also found on the same ALI day lower TEER in cells from asthmatic donors compared with non-asthmatic donors (Supplementary Fig. 2a), suggesting defective barrier function in those asthmatic cells. In uncompressed layers, we then examined how these differences in barrier function might correspond with changes in cellular jamming. Whether from non-asthmatic or asthmatic donors, the MSD and $\chi_4(\Delta t)$ showed that cells were highly motile and unjammed on early days in ALI culture (Fig. 2a,d and Supplementary Fig. 2b and Supplementary Movie 2). For example, on day 3 (Fig. 2g, triangles), HBECs from a non-asthmatic donor showed peaks in $\chi_4(\Delta t)$ indicative of faster-moving cooperative packs comprising roughly 20 cells with an average lifetime of 81 min, but by days 6 (Fig. 2g, circles) and 8 (Fig. 2g, asterisks), χ_4 (Δt) showed no peak, thus indicating that the layer had jammed.

Importantly, in cells from asthmatic donors compared with those from non-asthmatic donors this transition to the jammed phase in ALI culture was substantially delayed. For example, cells from a representative non-asthmatic donor jammed by day 6 (Fig. 2a–c,g and Supplementary Movie 2), whereas cells from a representative asthmatic donor became jammed only by day 14 (Fig. 2d–f,h and Supplementary Movie 3). On days 10 (Fig. 2h, circles) and 6 (Fig. 2h, triangles), HBECs from an asthmatic donor showed peaks in $\chi_4(\Delta t)$ indicative of faster-moving cooperative packs comprising approximately 26 and 12 cells with lifetimes of 72 and 90 min, respectively, but by day 14 (Fig. 2h, asterisks) showed no peaks in $\chi_4(\Delta t)$, thus indicating that the layer had jammed. This delayed jamming transition correlated well with delayed increases of TEER in cells from asthmatic donors compared with cells from non-asthmatic donors. For example, in cells from a representative non-asthmatic donor (Supplementary Fig. 2 and Supplementary Movie 2), TEER progressively increased to 370 Ω cm^2 by day 6 as cells jammed, and continued to increase to 700 Ω cm^2 until day 14, indicating that the early jamming transition corresponded to a rapid increase of barrier integrity. However, in cells from a representative asthmatic donor, TEER reached only 421 Ω cm^2 even on day 21 (Supplementary Fig. 2 and Supplementary Movie 3). Moreover, this delay in the spontaneous jamming transition was not donor specific, but was

consistently observed in cells obtained from multiple asthmatic donors compared with those from non-asthmatic donors acquired from the same source (The University of North Carolina, Methods; Supplementary Fig. 3). Whereas cells from all non-asthmatic donors (n = 5) became jammed between day 4 and 10 (Supplementary Fig. 3, blue circles), cells from asthmatic donors (n = 4) mostly remained unjammed as late as day 14 (Supplementary Fig. 3, red circles)

Together, these systematic changes in cooperative cellular motions establish that HBEC layers in ALI culture express spatially heterogeneous dynamics of the kind that in inert systems has been taken as being the signature of matter that is close to a jamming transition[23,26,27]. As shown below, all the epithelial systems studied here existed in the vicinity of a jamming transition[28]. It is already known that asthmatic HBECs exhibit an aberrant injury response and compromised differentiation[31], and here we demonstrate, further, that maturation of the airway epithelial layer coincides in time with the transition from an unjammed to a jammed condition, and that this transition is appreciably delayed in layers derived from asthmatic compared with non-asthmatic donors (Fig. 2).

Jamming and the adhesion paradox

In these collective cellular systems, what mechanical factors might promote cell jamming? Results from inert particulate matter[32,33] suggest that plausible mechanisms would include increased mutual crowding and increased mutual adhesion[4,9,16,17]. As regards mutual cellular crowding[34], we found no corresponding differences in the case of the marked hypermobility in cells from asthmatic versus non-asthmatic donors (Figs 1 and 2 and Supplementary Movies 1, 2 and 3). As regards mutual adhesion, we hypothesized that just as increased particle–particle adhesion promotes jamming in close-packed inert collective systems[7], so too increased cell–cell adhesion would promote jamming in the confluent living cellular layer[17]. Superficially at least, such a notion would help to explain why maturing HBEC layers derived from non-asthmatic donors tend to jam more rapidly than do those from asthmatic donors (Fig. 2 and Supplementary Fig. 3), and would be consistent with the observations that HBEC layers from asthmatic compared with non-asthmatic donors exhibit decreased TEER, increased permeability[30] and modestly diminished expression of E-cadherin[35]. We rejected this hypothesis, however, based on the experimental evidence described below.

In the confluent intact epithelial layer, tugging (tensile) stress transmitted across the cell–cell junction overwhelmingly dominates compressive stress[4,36]. As shown below, each cell tugs on immediate neighbours, but rarely pushes. Tugging stress exerted across the cell–cell junction can exist only to the extent that it is supported by cell–cell adhesive stress, there being no other mechanism to transmit tensile stress across a cell–cell junction. As such, we can logically equate tugging stress transmitted across the cell–cell junction to adhesive stress. To measure this adhesive stress within the intact cellular layer, we first used Monolayer Traction Microscopy to map local tractions that each cell exerts on its substrate, and then used Monolayer Stress Microscopy in the same layer to map intercellular stresses that each cell exerts on its immediate neighbours[4,8,36] (Methods). We plated primary HBECs obtained from non-asthmatic donors or from asthmatic donors (Fig. 3) on

apolyacrylamide gel (Young's modulus = 1.2 kPa, thickness = 100 μm); an important difference here compared with ALI culture conditions in Transwells described above is that plating HBECs on a gel precludes establishing an ALI culture. Hence, we resort to polyacrylamide only as a matter of necessity. Nonetheless, these HBECs showed cooperative fluctuations comparable to those described above for cells in ALI culture (Supplementary Fig. 4a,b). On day 3 after seeding, HBECs from three asthmatic donors showed peaks in $\chi_4(\Delta t)$ indicative of cooperative packs comprising approximately 80, 20 and 70 cells with lifetimes of 20, 30 and 40 min, respectively, but HBECs from non-asthmatic donors showed no peaks in $\chi_4(\Delta t)$, thus indicating that the layers had jammed (Supplementary Fig. 4c,d). In a representative layer derived from a non-asthmatic donor, tractions exerted by HBECs on the substrate fluctuated markedly in time and in space (Fig. 3a) on a scale comparable to but somewhat larger than the size of a cell. The intercellular stress was heterogeneous and predominantly tensile (Fig. 3c); in all experimental repetitions, stress averaged over the entire cell field was variable but tensile (average tension: 315 ± 283 Pa; $n = 5$). In the HBEC layers derived from asthmatic versus non-asthmatic donors, r.m.s. tractions exerted on the substrate were not statistically different, but tended to be larger (Fig. 3b,g; 114 ± 88 Pa versus 24 ± 7 Pa; $p = 0.22$). However, intercellular tensions exerted by each cell on its neighbours were larger by a factor 1.5 to 5 (Fig. 3d,h; 792 ± 171 Pa versus 257±82 Pa;$p = 0.02$). In both non-asthmatic and asthmatic HBECs, cells moved in packs, with regions of high tension (Fig. 3c,d) that spanned many cells (Fig. 3e,f), indicating that fluctuations in tension were cooperative over distances comparable to many cell diameters. To quantify the spatial extent of this stress cooperativity we measured the spatial autocorrelation function of tugging stress (tension), $C(R)$, as a function of cell separation distance, R (Methods). In every case the tension correlation $C(R)$ decayed over several hundred micrometres, but with faster spatial decay in cells derived from asthmatic versus non-asthmatic subjects (Fig. 3i; the correlation values $C(R)$ at 14μm were 0.29 ±0.02 and 0.48 ±0.03 in asthmatic and non-asthmatic HBEC layers, respectively; $p = 0.003$). HBECs derived from asthmatic versus non-asthmatic donors bear higher but more localized intercellular tension.

On the basis of these observations we cannot determine if buildup of intercellular adhesive stresses might promote unjamming or, conversely, if unjamming might promote build-up of intercellular adhesive stresses. We can say, however, that unjamming coexists with the amplification of local adhesive intercellular stresses, not with their attenuation (Fig. 3). This finding is counterintuitive, but is in concert nevertheless with comprehensive recent findings of others establishing by direct measurements that cell-cell adhesive stress is not attenuated by reducing the expression of E-cadherin[37].

Cell jamming, mutual adhesion and perimeter

To shed light on this paradox we turned to the vertex model of the cellular layer[18–20] (Supplementary Equations 1 and 2 in the Supplementary Information), which represents the projection of each cell in two-dimensions by an irregular curved polygon with a shape index, $p = P/\sqrt{A}$, where P and A *are* the cell perimeter and projected area, respectively (Supplementary Fig. 7). The model proposes that the mechanical energy associated with each cell is a function of three contributions: an energy associated with cell area and

attributable to area compressibility; an energy associated with cell perimeter attributable to the stiffness and contractility of the apical actomyosin ring; and an energy associated with interfaces of cell–cell contact, including the effects of adhesion molecules such as cadherins and associated actomyosin interactions, which, together, are expressible as a net line tension[14,20,38,39]. Whereas the first two contributions are always positive, the line tension decreases with increasing cell–cell adhesion or decreasing actin–myosin contractility, and therefore can be positive or negative[18,39]. These physical effects compete to generate a preferred cell shape, characterized by its preferred perimeter, p_0. In the vertex model cells can exchange places with immediate neighbours, but any such structural rearrangement requires changes in cell shapes. The change in energy required to complete such a structural rearrangement defines an energy barrier (Supplementary Fig. 7). Analysing this model, we find a scaling collapse in which the average energy barrier to structural rearrangements, $\Delta\varepsilon$, exhibits two critical branches,f_+ and f_-, as a function of the parameter p_0, with a crossover between them[19] at a critical value of p_0 denoted by p_0^*,

$$\Delta_\varepsilon = |p_0 - p_0^*|^\beta f_\pm(r|p_0 - p_0^*|^{-\Delta})$$

Here r is the reciprocal of perimeter stiffness (Supplementary Information), β and Δ are critical scaling exponents. Importantly, $p_0^* \cong 3.81$ is a critical shape index derived from the analysis of critical scaling behaviour; it is a pure number that rests on no adjustable model parameters or curve fitting to data[19] (Supplementary Information). As the argument of $f_\pm$ becomes small, one branch approaches a finite energy barrier height, thus implying solid-like behaviour with a finite shear modulus of the cellular collective. However, the other branch approaches a vanishing energy-barrier height and a vanishing shear modulus, thus implying no barrier to rearrangements and, therefore, unjammed fluid-like behaviour of the cellular collective. The former branch is predicted to prevail when $p_0 < p_0^*$ and the latter when $p_0 > p_0^*$.

To test further the prediction that cells in late ALI days were approaching a jammed state, we measured the shape index p for cells in HBEC layers as a function of ALI day in non-asthmatic and asthmatic HBECs (Methods); the median of p is denoted $\bar{p}$. Data indicate highly significant differences in $\bar{p}$ between ALI days, between cells derived from healthy versus asthmatic donors, and often between the observed value of $\bar{p}$ and the critical value 3.81 for jamming (Fig. 4 and Supplementary Fig. 5). However, as ALI day progressed, the structural parameter $\bar{p}$ progressively approached p_0^* (Fig. 4a and Supplementary Fig. 5). Note that because $\bar{p}$ is a measure of cellular structure, not cellular dynamics or intercellular stresses, it is independent of measurements of MSD, χ_4 and cellular stresses. As such, the behaviour in Fig. 4 independently validates the critical behaviour as jamming is approached, and implies that cells in the jammed state are unable to surmount the mechanical energy barriers that increase as cell–cell adhesion decreases (Supplementary Fig. 7). Importantly, in asthmatic compared with non-asthmatic HBECs, the approach of $\bar{p}$ to p_0^* is appreciably delayed. Moreover, after application of mechanical compressive stresses similar in magnitude to those expected during bronchospasm, the HBECs layer becomes unjammed and, as predicted from the vertex model, $\bar{p}$ substantially exceeds p_0^* (Supplementary Fig. 6).

Even for cells within the same epithelial layer, an important feature of the observed values of p for individual cells is their striking variability (Fig. 4 and Supplementary Fig. 5), which is much larger than measurement errors attributable to identification of cell boundaries derived from phase-contrast images. Geometry imposes some constraints on this variability; p, and therefore p, have no upper limit, but can never be smaller than the shape index for a circle, roughly 3.54. In the limit of vanishing active force fluctuations, as described here, the vertex model predicts the variability to be highly skewed[19] and to increase away from the critical point. Interestingly, the former of these predictions is borne out by observations, but the latter is not (Supplementary Fig. 5). As such, we suspected that active force fluctuations may contribute to the observed variability.

Therefore, we next incorporated small but non-negligible active-force fluctuations into the vertex model (Supplementary Information). Not surprisingly, increased force fluctuations are seen to work in concert with increased adhesion to unjam the cellular collective, providing another path to unjamming (Supplementary Movie 4). Cells in jammed model tissues fluctuate but do not change places with immediate neighbours, whereas structural rearrangements occur frequently in the unjammed tissue. Interestingly, such rearrangements cease and the model tissue becomes jammed when the shape index p approaches the same critical value of 3.81, regardless of the magnitude of the active fluctuations. This finding would explain why active HBECs still jam at $p = 3.81$, and suggests that the observed variability in p near the critical point might be attributable to active-force fluctuations. If true, then it may be possible in the future to estimate the properties of these active forces by comparing shape fluctuations predicted by active-vertex behaviour versus experimental observations. Another open question is the extent to which p can be used as a structural order parameter in other tissue types; finding that p is experimentally close to 3.81 is sufficient for an interpretation of a jammed state in our HBECs, which are isotropic in the plane. We expect that this analysis and this shape index may be useful for other isotropic tissues, but that it may fail in interesting and potentially predictable ways for anisotropic tissues, such as in the endothelial layer under shear flow[40].

The vertex model is therefore seen to capture essential features of collective cellular behaviour, especially the existence and properties of a jamming transition. Specifically, in some conditions each cell becomes frozen in place relative to immediate neighbours, as if caged, whereas in other conditions each cell readily exchanges places with immediate neighbours and, as a result, the integrated tissue continuously remodels. Concerning rates of cellular motion and rearrangement, across the transition there exist qualitative as well as quantitative differences in rates of cellular motion and rearrangement. The vertex model also predicts precisely how cell rearrangements across this transition—as independently assessed by dynamic metrics of jamming—are marked by changes in a specific index of cell shape (Fig. 4). Nevertheless, interesting theoretical questions remain unanswered. In the vertex model, for example, propulsive stresses are not taken explicitly into account. Theories based directly on self-propelled particles, by contrast, show that propulsive forces help to unjam particulate systems[3,41,42], but in such systems jamming is driven by mutual crowding rather than by changes in mutual adhesion or line tension. As such, they do not account for the changes of cell shape reported here, and they predict a transition that is therefore of a

fundamentally different kind (Supplementary Information)[43]. For that reason, addition of propulsive stresses to the vertex model would help to resolve the questions of the extent to which propulsive stresses might alter the nature of the transition or the centrality of the critical shape parameter, p_0^* (refs 20,39,44–46).

The emerging physical picture

It has been argued recently that a wide variety of living collective systems evolve spontaneously towards the neighbourhood of a critical phase transition[47–49]. In the particular case of the airway epithelial cellular layer, cellular motions (Figs 1 and 2), cellular forces (Fig. 3) and cellular shapes (Fig. 4) all provide strong evidence that a critical jamming transition occurs in these tissues. Our findings thereby suggest a new physical picture of airway epithelial remodelling, maturation and repair, in which epithelial cells migrate collectively in conditions close to a jamming transition[17]. When effective energy barriers are small or non-existent, the tissue is readily able to explore new configurations as the system remodels into new states, some of which might be adaptive and others maladaptive[9,16,17]. But, as energy barriers increase, the tissue becomes locked into a jammed state.

The bronchial epithelium is subject to repeated mechanical perturbations through the action of spontaneous breathing, and is subject to injury through exposure to harmful environmental pollutants, viruses, allergens, reactive oxygen species, or inflammatory mediators. Here we put forward the hypothesis that in non-asthmatic subjects these external factors can cause the cellular collective to unjam, explore various possible configurations, and then resettle into an adaptive quiescent, jammed, solid-like state; by so doing they effect self-repair in that remodelled state. Importantly, we have not yet determined the molecular mechanisms that impact the jamming transition, and we expect that there could be many. Nevertheless, the observations reported here establish a simple and easily measured structural index that quantifies the proximity of the layer to a jamming transition, and suggests that perhaps molecular mechanisms can be investigated and categorized by how they affect jamming.

Bronchial epithelial cells and their mechano-sensitivity are increasingly understood to play a major role in airway remodelling in asthma, but just how these events are linked to asthma pathobiology has remained unclear[1,12,14,15,21,34,50–52]. In cells from asthmatic compared with non-asthmatic donors in ALI culture, we show that the transition from a hypermobile, unjammed, fluid-like phase to a quiescent, jammed, solid-like phase is delayed substantially or disrupted altogether. Whether this delay arises from layer injury, immaturity, or dysmaturity, the prolonged or sustained hypermobile fluid-like phase defines an unanticipated maladaptive phenotype which, to our knowledge, comprises the first known instance—in any disease—where pathobiology is linked to the recent discovery of cellular jamming and unjamming[4,17,53,54]. It remains to be determined if these processes and their downstream effects might be favourably impacted by bronchodilators, corticosteroids, or other therapeutic interventions.

Methods

Methods and any associated references are available in the online version of the paper.

Methods

Culture of primary human bronchial epithelial cells

We used primary human bronchial epithelial cells (HBECs) derived from ten non-asthmatic and nine asthmatic donors from two distinct sources. Primary HBECs at passage 1 were purchased from Lonza or provided by S. Randell at the Marsico Lung Institute/Cystic Fibrosis Research Center at the University of North Carolina, Chapel Hill. Human lungs unsuitable for transplantation, including three cases of fatal asthma and one with asthma in the medical social history, were obtained under protocol #03–1396 approved by the University of North Carolina at Chapel Hill Biomedical Institutional Review Board. Informed consent was obtained from authorized representatives of all organ donors. All non-asthmatic lungs were from non-smokers with no history of chronic lung disease. HBECs from all donors were cultured as previously described[12]. Passage 2 HBECs were plated at a density of 125,000 cells cm^{-2} on 12-Transwell plates with polyester membranes with 0.4 μm pores (Corning) coated with 50 ng ml^{-1} of type 1 rat tail collagen (BD Biosciences). Cells were cultured for five to seven days under submerged conditions until confluence. Once cells reached confluence, submerged condition was switched to the ALI condition by removing medium from the apical surface. The ALI culture was maintained for another 16–18 days, unless described otherwise. By 10–11 days in ALI culture, cells from all donors produced a substantial amount of mucus at the apical surface.

Exposure of HBECs to compressive mechanical stress

On day 16 of ALI culture, when HBECs had matured into a well-differentiated phenotype of confluent bronchial epithelium similar to that existing *in vivo*[13], we exposed cells to apical-to-basal compressive stress spanning the physiologic ranges (0, 3, 10, 20, or 30 cm H_2O) for three hours as previously described[14,21,52], along with appropriate time-matched controls. For the comparison of cells from non-asthmatic versus asthmatic donors, we used cells on different ALI day, as indicated in Figs 2 and 4, during the course of ALI culture.

Measurement of cellular velocities in ALI culture

At 18 h after application of compressive stress, time-lapse phase-contrast images of HBECs in ALI culture were acquired on an inverted optical microscope (Leica, DMI 6000B) equipped with a heated (37°C), CO_2-controlled (5%), humidified chamber. For each condition and each donor, two to three wells were imaged at six different positions in each well at 3-min intervals for 150 min. In each region comprising roughly 1,200–1,500 well-differentiated cells, we mapped cellular motions within the pseudostratified layer in time and in space. Using phase-contrast images obtained in an apical focal plane, instantaneous cellular velocities were mapped by particle imaging velocimetry (PIV; refs 10,16) in which the cross-correlation window size was 64 × 64 pixels (pixel size of 0.44 μm). For each data set, the spatial distribution of cellular migration velocities was mapped based on a running boxcar average of instantaneous velocities throughout 150-min periods. Cellular trajectories

were computed by integration of the instantaneous velocity field obtained from the PIV, with interpolation of each displacement point to the nearest grid point. These trajectories closely approximate cellular motions[4,8,10,16,55]; to achieve accuracy comparable to individual cell tracking, we chose a grid spacing (3.5 μm) substantially smaller than the size of a single cell (15–20 μm).

Quantifying spatially heterogeneous dynamics of cellular motions

As a metric of cellular motions, mean square displacements (MSD) were computed as a function of time interval, Δ*t:*

$$\mathrm{MSD}(\Delta t)=\langle|\mathbf{r}_i(t+\Delta t)-\mathbf{r}_i(t)|^2\rangle$$

where $\mathbf{r}_i(t)$ indicates the position of cell i at time t and $\langle\ldots\rangle$ denotes the average over all time t, and all cells. The cellular self-diffusion coefficient defined as $D_s = \lim_{\Delta t\to\infty}\mathrm{MSD}(\Delta t)/(4\Delta t)$ was then computed. To quantify the dynamics of cellular motions, we computed the self-overlap order parameter[27]:

$$Q(\Delta t)=N^{-1}\sum_{i=1}^{N}w_i$$

where N is the number of cells and $w = 1$ if $|\mathbf{r}_i(t+\Delta t)-\mathbf{r}_i(t)| < 0.15d_c$ (where d_c is average cell diameter) and $w = 0$ otherwise. To quantify the size and lifetime of these cooperative fluctuations as proposed in ref. 24 proposed, spatially heterogeneous cellular dynamics in each sample were quantified by the four-point susceptibility χ_4, approximated by

$$\chi_4(\Delta t)=N[\langle Q(\Delta t)^2\rangle-\langle D(\Delta t)\rangle^2]$$

where N is the number of cells and $\langle\ldots\rangle$ denotes the ensemble average taken over all sequences of images and all time, t. This measure approximates the four-point susceptibility, $\chi_4(\Delta t)$, and possesses several useful attributes[4,27], such as quantitative measures of the size of cooperatively moving cell packs and their associated rearrangement times.

Measurement of mechanical stresses within the HBEC layer

To measure mechanical stresses within the layer plane, we seeded HBECs on a polyacrylamide gel (Youngs modulus = 1.2 kPa, thickness = 100 μm). Gel preparation and seeding protocols were similar to published protocols[4,10,54]. Briefly, we deposited a polydimethyl siloxane (PDMS) membrane with a rectangular opening (8×8 mm) on the gel. After coating the gel with type 1 collagen (BD Biosciences), we seeded HBECs derived from non-asthmatic and asthmatic subjects. We then removed the PDMS membrane and allowed HBECs to grow to confluence for three days. Fluorescence and phase-contrast images were acquired at 10-min intervals for 2 h. Local gel displacements were quantified from an image of embedded fluorescent markers at each experimental time point and a reference image obtained after trypsinization. Local migration velocities and gel

displacements were obtained by the PIV method[10,16] using a cross-correlation window size of 32 ×32 pixels (pixel size of 0.88 μm). To obtain substrate tractions, we used the numerical procedure from Fourier-Transform Traction Microscopy[10,56]. To obtain layer stresses, we used the numerical procedure from Monolayer Stress Microscopy[4,36,54]. Briefly, we computed a map of the tractions exerted by the cells on their substrate using gel displacements. From these tractions, we obtained the distribution of intercellular stresses within the cellular sheet. At each point in the cellular sheet, we computed the two principal stress components σ_{max} and σ_{min} and their corresponding, mutually perpendicular, principal orientations. We then computed the local tension within the cellular sheet, defined as $\bar{\sigma} = (\sigma_{max} + \sigma_{min})/2$. The boundary edge of the patterned cellular sheet was taken to be zero stress[4,36]. After recovery of a stress map, an area near the edge (∼1 mm) was cropped from the map (Fig. 3a – d).

Calculation of the spatial autocorrelation function of tension

To quantify the spatial extent of stress cooperativity, we computed the spatial autocorrelation function of intercellular tension[4]:

$$C(R)=\frac{1}{N\mathrm{var}(\bar{\sigma})}\sum_{i,j=1}^{N}\left[\sum_{|R_i-R_j|=R}\delta\bar{\sigma}_i\delta\bar{\sigma}_i\right]$$

where $\delta\bar{\sigma}_i$ is the local departure of the tension at position R_i from its spatial mean $\langle\bar{\sigma}\rangle$, $\mathrm{var}(\bar{\sigma})$ is the variance of those departures, and the $|R_i - R_j| = R$ denotes equality within a uniform bin width of 20 μm, within which there are N points.

Quantification of cell shapes in ALI culture

Time-lapse phase-contrast images of HBECs in ALI culture were acquired as described above. For each condition and donor, 130 cells were manually traced using ImageJ software (National Institutes of Health) from four different fields of view, and the shape index $p=P/\sqrt{A}$, where P and A are the cell perimeter and projected area, was computed for each traced cell. The median of this shape parameter $\bar{p}$ was computed. With a'bootstrap' method[57], the data were uniformly randomly sampled with replacement 10^5 times, from which the distribution of the resulting medians was used to determine confidence intervals and p-values.

Supplementary Material

Refer to Web version on PubMed Central for supplementary material.

Acknowledgements

Authors thank the staff of the UNC CF Center, Tissue Procurement and Cell Culture Core at the University of North Carolina, Chapel Hill. This research was supported by the Francis Family Foundation, the Alfred P. Sloan Foundation, the American Heart Association (13SDG14320004), the National Research Foundation of Korea (NRF-2013S1A2A2035518), the National Science Foundation (BMMB-1334611, DMR-1352184) and the National Institutes of Health (K25HL091124, P30DK065988, P30ES000002, HL007118, R01HL102373, R01HL107561, P01HL120839).

References

1. Holgate ST. Pathogenesis of asthma. Clin. Exp. Allergy. 2008; 38:872–897. [PubMed: 18498538]
2. Friedl P, Gilmour D. Collective cell migration in morphogenesis, regeneration and cancer. Nature Rev. Mol. Cell Biol. 2009; 10:445–457. [PubMed: 19546857]
3. Henkes S, Fily Y, Marchetti MC. Active jamming: Self-propelled soft particles at high density. Phys. Rev E. 2011; 84:040301.
4. Tambe DT, et al. Collective cell guidance by cooperative intercellular forces. Nature Mater. 2011; 10:469–475. [PubMed: 21602808]
5. Haeger A, Krause M, Wolf K, Friedl P. Cell jamming: Collective invasion of mesenchymal tumor cells imposed by tissue confinement. Biochim. Biophys. Acta. 2014; 1840:2386–2395. [PubMed: 24721714]
6. Thiery JP, Acloque H, Huang RY, Nieto MA. Epithelial-mesenchymal transitions in development and disease. Cell. 2009; 139:871–890. [PubMed: 19945376]
7. Banigan EJ, Illich MK, Stace-Naughton DJ, Egolf DA. The chaotic dynamics of jamming. Nature Phys. 2013; 9:288–292.
8. Kim JH, et al. Propulsion and navigation within the advancing monolayer sheet. Nature Mater. 2013; 12:856–863. [PubMed: 23793160]
9. Nnetu K, Knorr M, Pawlizak S, Fuhs T, Käs JA. Slow and anomalous dynamics of an MCF-10A epithelial cell monolayer. Soft Matter. 2013; 9:9335–9341.
10. Trepat X, et al. Physical forces during collective cell migration. Nature Phys. 2009; 5:426–430.
11. Berthier L. Nonequilibrium glassy dynamics of self-propelled hard disks. Phys. Rev. Lett. 2014; 112:220602. [PubMed: 24949749]
12. Park JA, Tschumperlin DJ. Chronic intermittent mechanical stress increases MUC5AC protein expression. Am. J. Respir. Cell Mol. Biol. 2009; 41:459–466. [PubMed: 19168703]
13. Gray TE, Guzman K, Davis CW, Abdullah LH, Nettesheim P. Mucociliary differentiation of serially passaged normal human tracheobronchial epithelial cells. Am. J. Respir. Cell Mol. Biol. 1996; 14:104–112. [PubMed: 8534481]
14. Tschumperlin DJ, et al. Mechanotransduction through growth-factor shedding into the extracellular space. Nature. 2004; 429:83–86. [PubMed: 15103386]
15. Grainge CL, et al. Effect of bronchoconstriction on airway remodeling in asthma. N. Engl. J. Med. 2011; 364:2006–2015. [PubMed: 21612469]
16. Angelini TE, et al. Glass-like dynamics of collective cell migration. Proc. Natl Acad. Sci. USA. 2011; 108:4714–4719. [PubMed: 21321233]
17. Sadati M, Taheri Qazvini N, Krishnan R, Park CY, Fredberg JJ. Collective migration and cell jamming. Differentiation. 2013; 86:121–125. [PubMed: 23791490]
18. Farhadifar R, Roper JC, Aigouy B, Eaton S, Julicher F. The influence of cell mechanics, cell-cell interactions, and proliferation on epithelial packing. Curr. Biol. 2007; 17:2095–2104. [PubMed: 18082406]
19. Bi, D.; Lopez, J.; Schwarz, J.; Manning, ML. A density-independent glass transition in biological tissues. 2014. Preprint at http://arXiv.org/abs/1409.0593v1
20. Bi D, Lopez JH, Schwarz JM, Manning ML. Energy barriers and cell migration in densely packed tissues. Soft Matter. 2014; 10:1885–1890. [PubMed: 24652538]
21. Wiggs BR, Hrousis CA, Drazen JM, Kamm RD. On the mechanism of mucosal folding in normal and asthmatic airways. J. Appl. Phys. 1997; 83:1814–1821.
22. Gunst SJ, Stropp JQ. Pressure-volume and length-stress relationships in canine bronchi *in vitro* . J. Appl. Phys. 1988; 64:2522–2531.
23. Keys A, Abate A, Glotzer SC, Durian DJ. Measurement of growing dynamical length scales and prediction of the jamming transition in granular material. Nature Phys. 2007; 3:260–264.
24. Berthier L, et al. Direct experimental evidence of a growing length scale accompanying the glass transition. Science. 2005; 310:1797–1800. [PubMed: 16357256]

25. Weeks ER, Crocker JC, Levitt AC, Schofield A, Weitz DA. Three-dimensional direct imaging of structural relaxation near the colloidal glass transition. Science. 2000; 287:627–631. [PubMed: 10649991]
26. Garrahan JP. Dynamic heterogeneity comes to life. Proc. Natl Acad. Sci. USA. 2011; 108:4701–4702.
27. Abate AR, Durian DJ. Topological persistence and dynamical heterogeneities near jamming. Phys. Rev. E. 2007; 76:021306.
28. Angell CA. Formation of glasses from liquids and biopolymers. Science. 1995; 267:1924–1935. [PubMed: 17770101]
29. Damera G, et al. Ozone modulates IL-6 secretion in human airway epithelial and smooth muscle cells. Am. J. Physiol. Lung Cell Mol. Physiol. 2009; 296:L674–L683. [PubMed: 19201813]
30. Xiao C, et al. Defective epithelial barrier function in asthma. J. Allergy Clin. Immunol. 2011; 128:549–556. [PubMed: 21752437]
31. Roth HM, Wadsworth SJ, Kahn M, Knight DA. The airway epithelium in asthma: Developmental issues that scar the airways for life? Pulm. Pharmacol. Ther. 2012; 25:420–426. [PubMed: 23022283]
32. Trappe V, Prasad V, Cipelletti L, Segre PN, Weitz DA. Jamming phase diagram for attractive particles. Nature. 2001; 411:772–775. [PubMed: 11459050]
33. Liu AJ, Nagel SR. Jamming is not just cool any more. Nature. 1998; 396:21–22.
34. Park JA, Drazen JM, Tschumperlin DJ. The chitinase-like protein YKL-40 is secreted by airway epithelial cells at base line and in response to compressive mechanical stress. J. Biol. Chem. 2010; 285:29817–29825. [PubMed: 20650887]
35. Hardyman MA, et al. TNF-α-mediated bronchial barrier disruption and regulation by src-family kinase activation. J. Allergy Clin. Immunol. 2013; 132:665–672. [PubMed: 23632299]
36. Tambe DT, et al. Monolayer stress microscopy: Limitations, artifacts, and accuracy of recovered intercellular stresses. PLoS ONE. 2013; 8:55172.
37. Bazellieres E, et al. Control of cell-cell forces and collective cell dynamics by the intercellular adhesome. Nature Cell Biol. 2015; 17:409–420. [PubMed: 25812522]
38. Glazier JA, Graner F. Simulation of the differential adhesion driven rearrangement of biological cells. Phys. Rev. E. 1993; 47:2128–2154.
39. Brodland GW. The differential interfacial tension hypothesis (DITH): A comprehensive theory for the self-rearrangement of embryonic cells and tissues. J. Biomech. Eng. 2002; 124:188–197. [PubMed: 12002128]
40. Steward R, Tambe D Jr, Hardin CC, Krishnan R, Fredberg JJ. Fluid shear, intercellular stress, and endothelial cell alignment. Am. J. Physiol. Cell Physiol. 2015; 308:C657–C664. [PubMed: 25652451]
41. Yang X, Manning ML, Marchetti MC. Aggregation and segregation of confined active particles. Soft Matter. 2014; 10:6477–6484. [PubMed: 25046587]
42. Basan M, Elgeti J, Hannezo E, Rappel WJ, Levine H. Alignment of cellular motility forces with tissue flow as a mechanism for efficient wound healing. Proc. Natl Acad. Sci. USA. 2013; 110:2452–2459. [PubMed: 23345440]
43. Sepulveda N, et al. Collective cell motion in an epithelial sheet can be quantitatively described by a stochastic interacting particle model. PLoS Comput. Biol. 2013; 9:1002944.
44. Szabo A, et al. Collective cell motion in endothelial monolayers. Phys. Biol. 2010; 7:046007. [PubMed: 21076204]
45. Kabla AJ. Collective cell migration: Leadership, invasion and segregation. J. R. Soc. Interface. 2012; 9:3268–3278. [PubMed: 22832363]
46. Li B, Sun SX. Coherent motions in confluent cell monolayer sheets. Biophys. J. 2014; 107:1532–1541. [PubMed: 25296305]
47. Attanasi A, et al. Finite-size scaling as a way to probe near-criticality in natural swarms. Phys. Rev. Lett. 2014; 113:238102. [PubMed: 25526161]
48. Fredberg JJ. Power steering, power brakes, and jamming: Evolution of collective cell-cell interactions. Physiology. 2014; 29:218–219. [PubMed: 24985324]

49. Hidalgo J, et al. Information-based fitness and the emergence of criticality in living systems. Proc. Natl Acad. Sci. USA. 2014; 111:10095–10100. [PubMed: 24982145]
50. Lazaar AL, Panettieri RA. Jr Is airway remodeling clinically relevant in asthma? Am. J. Med. 2003; 115:652–659. [PubMed: 14656618]
51. Swartz MA, Tschumperlin DJ, Kamm RD, Drazen JM. Mechanical stress is communicated between different cell types to elicit matrix remodeling. Proc. Natl Acad. Sci. USA. 2001; 98:6180–6185. [PubMed: 11353845]
52. Park JA, et al. Tissue factor-bearing exosome secretion from human mechanically stimulated bronchial epithelial cells *in vitro* and *in vivo* . J. Allergy Clin. Immunol. 2012; 130:1375–1383. [PubMed: 22828416]
53. Trepat X, et al. Universal physical responses to stretch in the living cell. Nature. 2007; 447:592–595. [PubMed: 17538621]
54. Serra-Picamal X, et al. Mechanical waves during tissue expansion. Nature Phys. 2012; 8:628–634.
55. Angelini TE, Hannezo E, Trepat X, Fredberg JJ, Weitz DA. Cell migration driven by cooperative substrate deformation patterns. Phys. Rev. Lett. 2010; 104:168104. [PubMed: 20482085]
56. Butler JP, Tolic-Norrelykke IM, Fabry B, Fredberg JJ. Traction fields, moments, and strain energy that cells exert on their surroundings. Am. J. Physiol Cell Physiol. 2002; 282:C595–C605. [PubMed: 11832345]
57. Efron, B.; Tibshirani, R. An Introduction to the Bootstrap. Chapman & Hall; 1993.

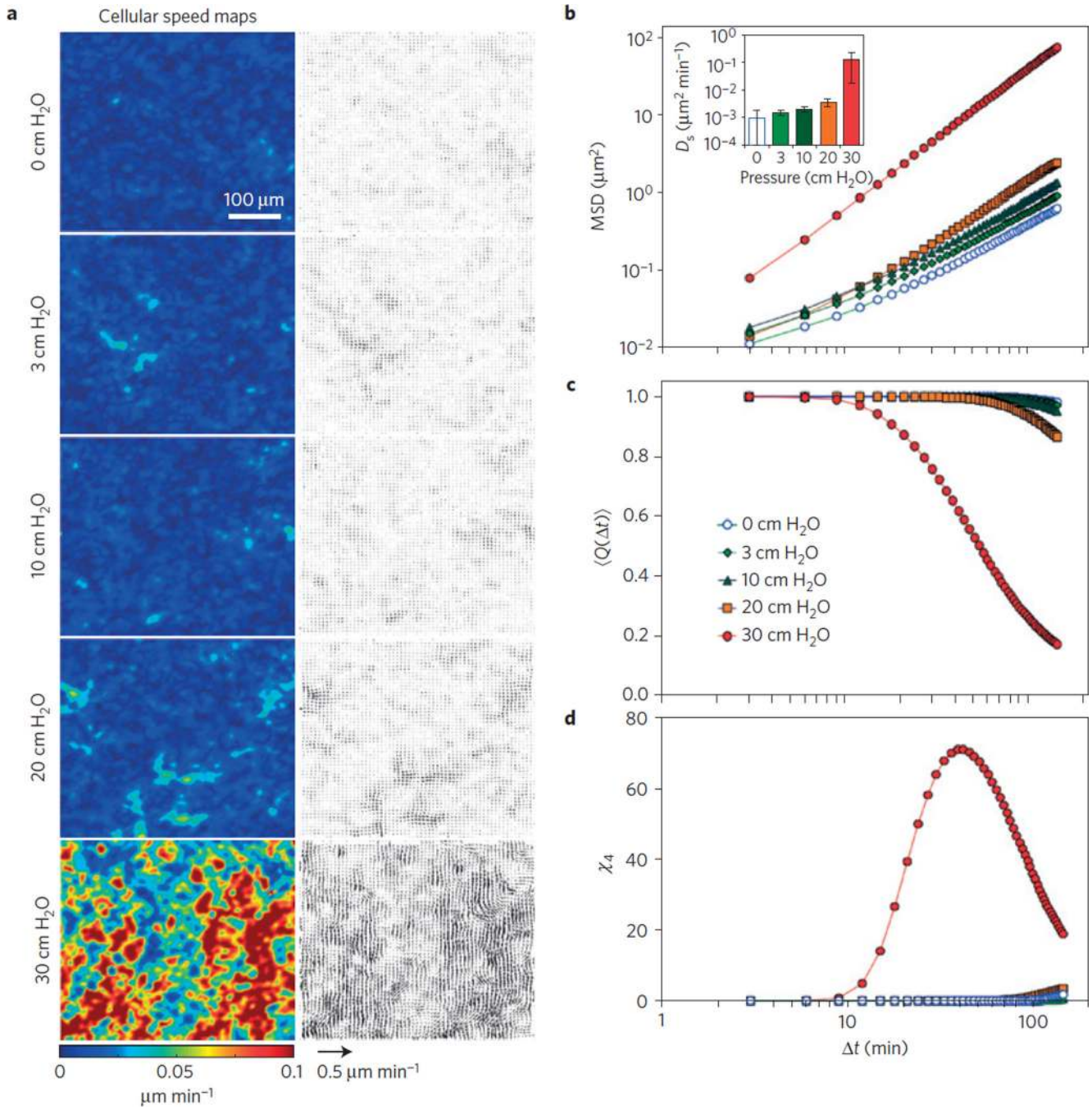

Figure 1. In a confluent layer of well-differentiated HBECs, compressive stress mimicking bronchospasm, as in asthmatic bronchospasm, provokes the transition from a solid-like jammed phase to a fluid-like unjammed phase

a, Speed maps (left panels) showed compressive stress at a magnitude of 30 cm H_2O induced hypermobility of HBECs on ALI day 16. Within any optical field the migration speed was spatially heterogeneous but increased strongly with increasing *P*. Colour scale is shown at the bottom of the left panels. The size of vectors (right panels) increased with increasing *P* and showed large-scale dynamic heterogeneity. Vector scale is shown at the bottom of the right panels. **b**, As *P* was progressively increased to 30 cm H_2O (red filled

circles), the mean square displacement, MSD, and the self-diffusion coefficient D_s increased (inset; $D_s = \lim_{\Delta t \to \infty} \mathrm{MSD}(\Delta t)/(4\Delta t)$), and the system became strongly super-diffusive. Error bars in the inset represent the standard deviation. **c**, When P was less than 20 cm H_2O, the relative overlap of each cell with its initial position was nearly perfect for time intervals (Δt) of less than 144 min, as quantified by the ensemble average, $\langle Q(\Delta t) \rangle$, close to 1. When P was 30 cm H_2O (red filled circles), the overlap decreased to 0.17. **d**, The four-point susceptibility $\chi_4(\Delta t)$ is approximated by $N[\langle Q(\Delta t)^2 \rangle - \langle Q(\Delta t) \rangle^2]$, where N is the number of cells. When movements are cooperative, $\chi_4(\Delta t)$ exhibits a peak whose position corresponds roughly to pack lifetime, and whose magnitude corresponds roughly to pack size. When pressure was 30 cm H_2O (red filled circles), $\chi_4(\Delta t)$ showed a peak indicative of cooperative packs of faster-moving cells with a pack lifetime of 45 min and a pack size of approximately 70 cells.

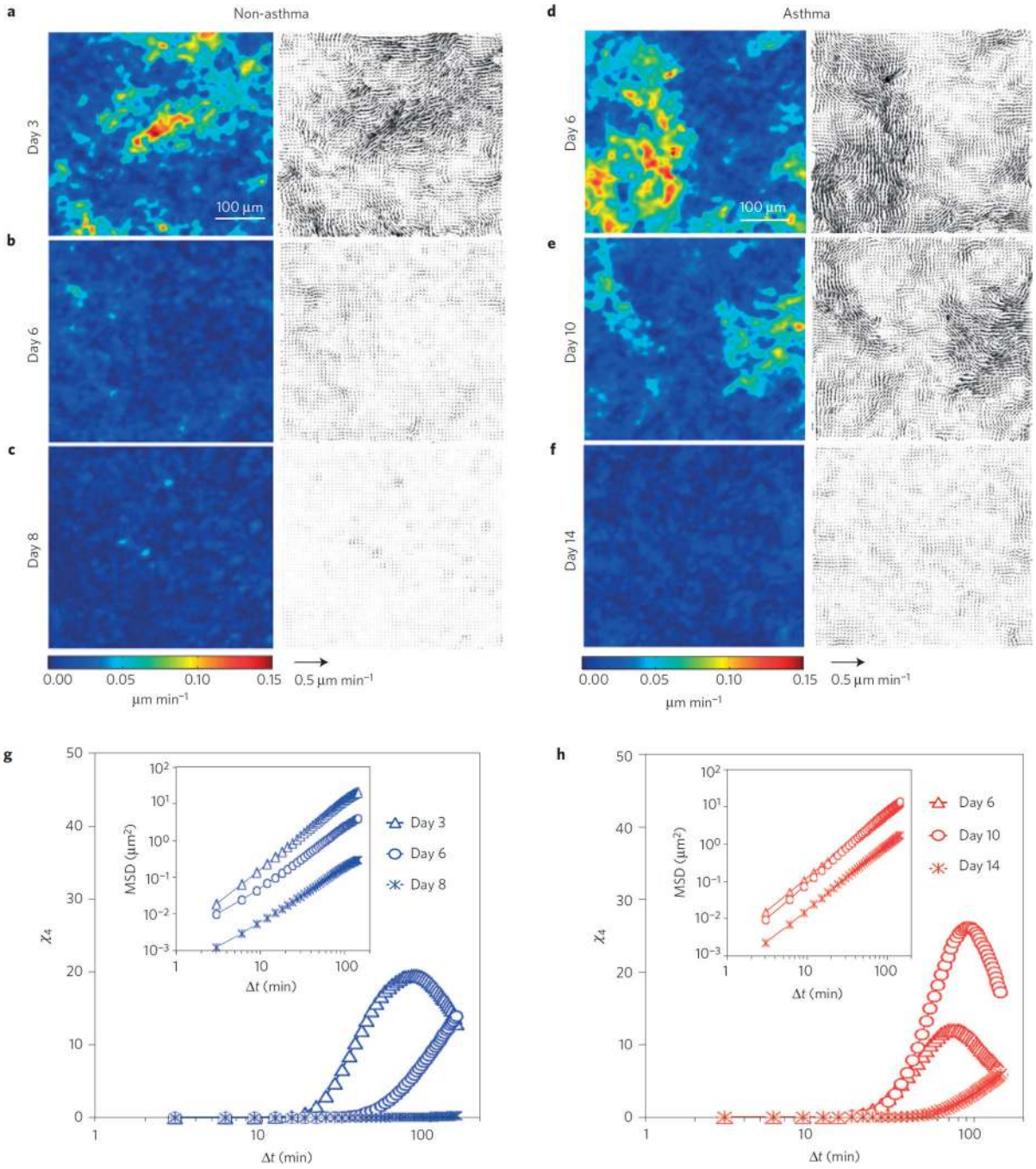

Figure 2. In HBECs over the course of ALI culture, a spontaneous phase transition occurs from a hypermobile, unjammed, fluid-like phase into a quiescent, jammed, solid-like phase, which was delayed in cells from asthmatic donors

a–c, Speed maps (left panels) and vector maps (right panels) showed that HBECs from a representative non-asthmatic donor were hypermobile on an early ALI day (**a**; day 3), but spontaneously became quiescent on later ALI days (**b**, day 6; and **c**, day 8). Colour and vector scales are shown at the bottom of **c. d–f**, Speed maps (left panels) and vector maps (right panels) showed that HBECs from a representative asthmatic donor were hypermobile until later ALI days (**d**, day 6; and **e**, day 10) and became quiescent on ALI day 14 (**f**).

Colour and vector scales are shown at the bottom of **f. g**, Four-point susceptibility $\chi_4(\Delta t)$ for HBECs from a non-asthmatic donor showed peaks indicative of cooperative packs of faster-moving cells with a lifetime of 81 min with a corresponding pack size of approximately 20 cells on ALI day 3 (blue triangles), whereas peak was undetectable either on ALI day 6 (blue circles) or 8 (blue asterisks). Inset: MSD. **h**, Four-point susceptibility $\chi_4(\Delta t)$ for HBECs from an asthmatic donor showed peaks indicative of cooperative packs of faster-moving cells with lifetimes of 72 and 90 min with corresponding pack sizes of approximately 26 and 12 cells on ALI day 10 (red circles) and 6 (red triangles), respectively, whereas peak was undetectable on ALI day 14 (red asterisks). Inset: MSD.

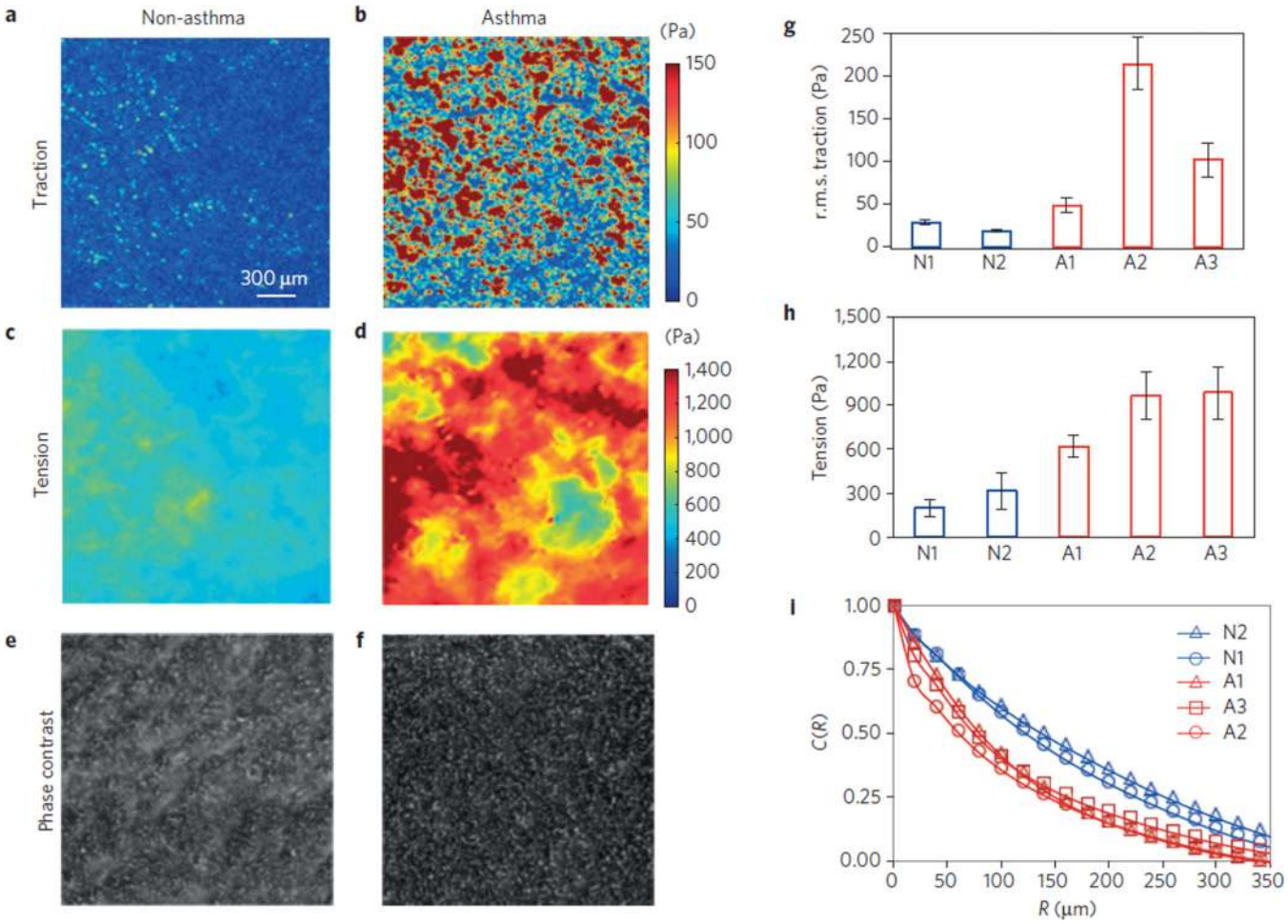

Figure 3. In HBECs derived from asthmatic donors compared with those from non-asthmatic donors, tractions and intercellular stresses are greater but the spatial correlation of tension decays faster

a,b, Colour maps of tractions exerted by HBECs derived from a non-asthmatic donor (**a**; N2 in **g–i**) and an asthmatic donor (**b**; A2 in **g–i**) on their substrates. Colour scale is shown to the right of **b. c,d**, Colour maps of intercellular stresses exerted across cell–cell junctions for donors N2 (**c**) and A2 (**d**) show packs of high tension that span many cell diameters. Colour scale is shown to the right of **d. e,f**, Phase-contrast maps of HBEC layers on polyacrylamide gels for donors N2 (**e**) and A2 (**f**). **g**, In cells derived from asthmatic donors (red: A1, A2, A3) versus non-asthmatic donors (blue: N1, N2), root mean square (r.m.s.) tractions were not statistically different, but tended to be larger (r.m.s. traction: 114±88 Pa versus 24±7 Pa; variance: 7,821 versus 53; $p = 0.22$). **h**, Intercellular tensions were larger by a factor of 1.5 to 5 in cells derived from asthmatic (red) versus non-asthmatic donors (blue; tension: 792 ±171 Pa versus 257±82 Pa; variance: 29,426 versus 6,787; $p = 0.02$). **i**, Spatial autocorrelation function, $C(R)$, of tension as a function of cell separation distance, R, shows that the tension correlation decayed over several hundred micrometres in all cases, but extended to shorter distances in cells derived from asthmatic (red symbols) versus non-asthmatic donors (blue symbols), thus confirming that intercellular stresses were larger in magnitude but more highly localized in the HBECs derived from asthmatic donors

compared with non-asthmatic donors ($C(R)$ at 140 μm in asthmatic versus non-asthmatic HBEC layers: 0.29±0.02 versus 0.48±0.03; variance: 0.0004 versus 0.0009; $p = 0.003$). The r.m.s. tractions, intercellular tensions and spatial autocorrelation in **g–i** were averaged across three to five experimental repeats for each donor. Error bars in **g,h** represent the standard error.

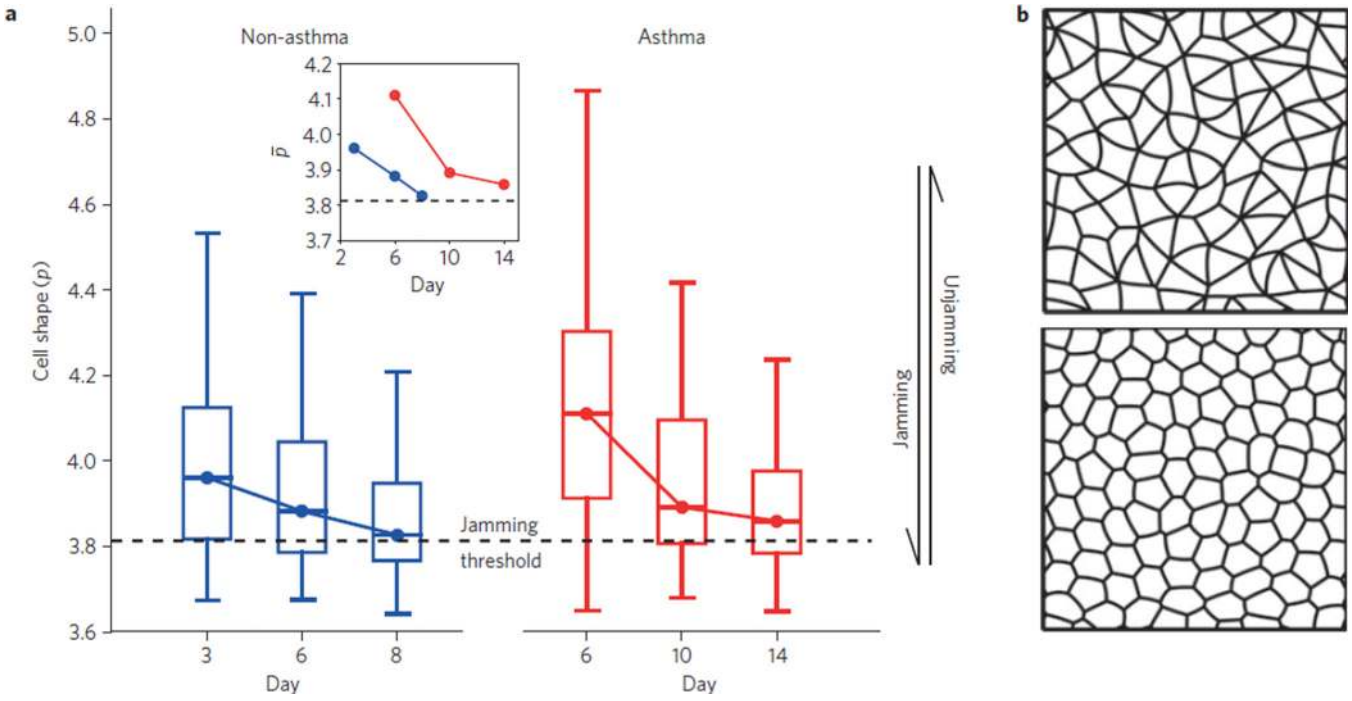

Figure 4. With increasing maturation of HBECs in ALI culture, cell perimeter, as expressed by the non-dimensional parameter p, decreases systematically towards the critical value p_0^* (3.81) predicted to occur at jamming by the vertex model together with the theory of critical scaling exponents

a, Over the course of maturation in ALI culture, HBECs from a representative non-asthmatic donor (Fig. 2 and Supplementary Movie 2) approached the jammed state, and the median ratio of perimeter to the square root area of cells systematically approached the jamming threshold p_0^*. In HBECs from a representative asthmatic donor (Fig. 2 and Supplementary Movie 3), however, the approach of p to p_0^* was considerably delayed. Over time, and in both cases, p systematically approached the jamming threshold of 3.81. Inset: p for representative non-asthmatic and asthmatic donors plotted with the same axis of ALI days to allow comparison of the jamming transition timing. Boxplot shows median and quartiles. Whiskers are maximum and minimum data points. **b**, Simulated tissues with input parameters of target cell-shape index p_0 =4.2, corresponding to a fluidized state (top panel), and p_0 =3.813, corresponding to a jammed tissue (bottom panel).